ACS OMEGA

http://pubs.acs.org/journal/acsodf

Article

# Click Chemistry-Generated Auristatin F–Linker–Benzylguanine for a SNAP-Tag-Based Recombinant Antibody–Drug Conjugate Demonstrating Selective Cytotoxicity toward EGFR-Overexpressing Tumor Cells

Allan M. Huysamen, Olaolu E. Fadeyi, Grace Mayuni, Dennis M. Dogbey, Neelakshi Mungra, Fleury A. N. Biteghe, Natasha Hardcastle, Dharanidharan Ramamurthy, Olusiji A. Akinrinmade, Krupa Naran, Susan Cooper, Dirk Lang, Wolfgang Richter, Roger Hunter,*,◆ and Stefan Barth*,◆

Cite This: *ACS Omega* 2023, 8, 4026–4037

Read Online

ACCESS | Metrics & More | Article Recommendations | Supporting Information

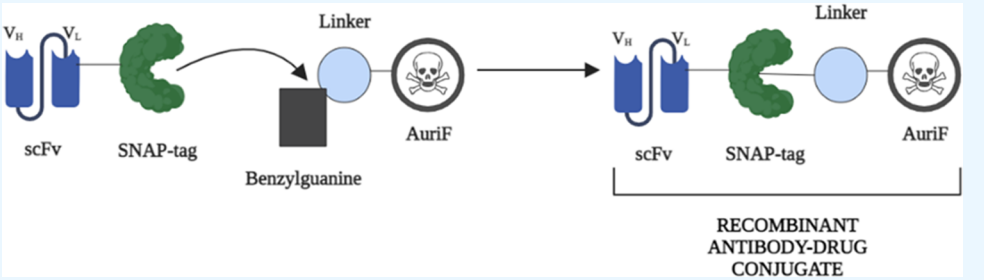


**ABSTRACT:** Antibody–drug conjugates (ADCs) are bifunctional molecules combining the targeting potential of monoclonal antibodies with the cancer-killing ability of cytotoxic drugs. This simple yet intelligently designed system directly addresses the lack of specificity encountered with conventional anti-cancer treatment regimes. However, despite their initial success, the generation of clinically sustainable and effective ADCs has been plagued by poor tumor penetration, undefined chemical linkages, unpredictable pharmacokinetic profiles, and heterogeneous mixtures of products. To this end, we generated a SNAP-tag-based fusion protein targeting the epidermal growth factor receptor (EGFR)—a biomarker of aggressive and drug-resistant cancers. Here, we demonstrate the use of a novel click coupling strategy to engineer a benzylguanine (BG)–linker–auristatin F (AuriF) piece that can be covalently tethered to the EGFR-targeting SNAP-tag-based fusion protein in an irreversible 1:1 stoichiometric reaction to form a homogeneous product. Furthermore, using these recombinant ADCs to target EGFR-overexpressing tumor cells, we provide a proof-of-principle for generating biologically active antimitotic therapeutic proteins capable of inducing cell death in a dose-dependent manner, thus alleviating some of the challenges of early ADC development.

## INTRODUCTION

The epidermal growth factor receptor (EGFR) is a member of the transmembrane tyrosine kinase receptor family (HER), comprising an extracellular ligand binding domain (EC), a transmembrane domain (TM), and an intracellular domain with tyrosine function.[1,2] EGFR activation starts with ligand binding that triggers dimerization (homo- and/or heterodimerization), which leads to tyrosine kinase domain autophosphorylation. In turn, this activates a cascade of downstream signaling pathways such as the RAS/MAPK, PI3K/Akt, Jak/Stat, and activator-of-transcription 3 (STAT3) pathway, all of which are implicated in the transcriptional regulation of genes involved in cell proliferation, cell survival, migration, and drug resistance.[1−3] As a result, novel therapeutic strategies in the form of anti-EGFR monoclonal antibodies (mAbs) and tyrosine kinase inhibitors (TKIs) (e.g., gefitinib and erlotinib) have been developed.[4−8] These therapies work respectively by obstructing EGFR binding with agnostic ligands (mAbs) and by suppressing the intracellular tyrosinase activity through disruption of adenosine-5′-triphosphate (ATP) binding (TKIs).[4−8] The clinical success of these therapies was demonstrated by the FDA approval of erlotinib (2004) and gefitinib (2015) for the treatment of non-small-cell lung cancer (NSCLC), and cetuximab (approved in 2004) and panitumumab (2006) mAbs for treating colorectal cancer.[4,5,7,8] However, these (cetuximab and panitumumab) are yet to demonstrate palpable therapeutic benefits, as they only

Received: October 24, 2022
Accepted: January 3, 2023
Published: January 17, 2023

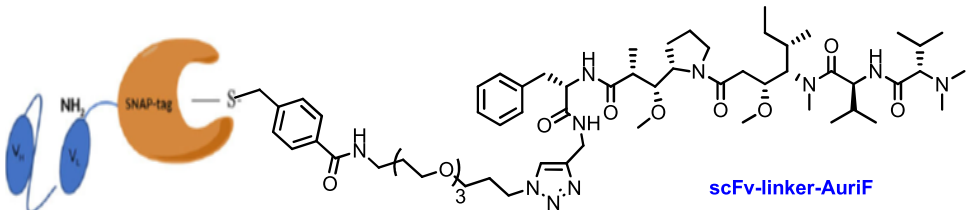


**Figure 1.** Structure of ADC target, scFv−linker−AuriF. The structure of the recombinant ADC target containing a scFv bonded to a relatively short linker containing a triazole generated from the click chemistry followed by AuriF as an amide at its C-end with a dimethylamino N-terminus.

achieve significant therapeutic efficacies when combined with systemic chemotherapy or radiotherapy and TKIs but not when used as monotherapy.[7−10] Therefore, efforts to mitigate these suboptimal therapeutic effects have paved the way for the development of antibody−drug conjugates (ADCs), a fast-growing type of biotherapeutic[9] with the potential to increase the antitumor activity of an antibody.[1,9−14] These ADCs typically comprise a mAb serving as a vehicle that selectively recognizes cancer cells overexpressing cognate cell surface receptors in comparison to normal cells. Upon recognition through ligand−receptor binding, the mAb enters the cell to specifically deliver the cytotoxic molecule, which subsequently induces cell death in cancer cells but not in normal cells.[1,9−11]

Indeed, the field of ADCs involving recombinant antibodies has become a proven modality for targeted cancer chemotherapy, with nine clinically approved ADCs as of 2021. Important examples include gemtuzumab ozogamicin and brentuximab vedotin, which were FDA-approved in 2000 and 2011, respectively, and contain full immunoglobulin (IgG) antibodies. This field has been extensively reviewed regarding both the chemistry of the antibody−linker−payload construct as well as its biology.[15−17] However, several constraints remain for IgG-based ADCs, including chemical instability toward storage, low blood residency and penetration capacity to the tumor microenvironment, a low payload potency, immunogenicity issues, off-target toxicity, as well as drug resistance.[15−18] In addition, early methods of antibody payload attachment chemistry (via lysine or cysteine amino and thiol groups, respectively) resulted in an uncertain and heterogeneous drug-to-antibody ratio (DAR), which, when greater than 4, results in antibody aggregates, a lower tolerated dose, and a faster systemic clearance; conversely, a lower DAR suffers from low drug efficacy.

The advances and limitations of ADCs for cancer therapy based on IgGs have been recently reviewed.[18] In response to these limitations, researchers have recently directed their attention to using smaller protein fragments (<75 kDa) as alternative antibodies to IgGs (150 kDa), particularly to meet the challenges presented in treating solid tumors.[19] One of these in the 25−30 kDa range are the single chain fragment variables (scFvs) comprising the IgG antigen binding Fv regions of the heavy ($V_H$) and light ($V_L$) chains joined together by a flexible peptide spacer of ∼25 amino acids in length. The much smaller size of the scFvs results in superior tumor penetration, while their lack of an Fc region ensures that interactions with off-target Fc-positive receptor cells is negated, thus reducing toxicity. However, these improvements must be counterbalanced against a shorter half-life and bioavailability window, resulting in reduced overall uptake.[19]

A limited number of scFvs from research laboratories have appeared in an ADC context in recent years, and a major advantage of this approach is the site-specific conjugation to a tether-payload moiety that can be achieved, resulting in a predictive DAR (1:1) to ensure the production of a homogeneous ADC with reduced toxicity compared to IgG-based ADCs. One such approach is to recombinantly engineer a SNAP-tag domain into any of the termini of the scFv.[20−27] This domain, which mimics the human DNA repair enzyme $O^6$-alkylguanine-DNA alkyltransferase (hAGT), contains a thiolate nucleophile that can be alkylated by a methylene (on the end of the linker) bearing an $O^6$-benzylguanine (BG) leaving group, thus producing homogeneous ADC conjugates with reproducible 1:1 stoichiometry. To date, there have been few examples reported in the literature of promising scFv-based ADCs using SNAP-tag conjugation methodology.[12,14−16,28,29] Furthermore, although, to date, click chemistry is known for linker connection chemistry in IgG-based ADCs, to the best of our knowledge, there are no reports of using a click strategy for linker connection to a scFv.[30−32] This facet features as a novel aspect of the present work in that we have achieved the first click strategy for assembling an scFv-based ADC involving a noncleavable linker, whose characteristics are reviewed below. Our strategy affords a relatively facile means of modular assembly for accessing a library of scFv-based ADC structural variants.

Previous studies conducted by Woitok et al. reported the targeted therapeutic potential of panitumumab- and cetuximab-derived 1711/425 scFv-SNAP-tag fusion proteins in specifically detecting and killing EGFR-expressing breast and skin cancer cells while sparing the receptor-negative cells, using nanomolar range concentrations of the small molecule toxins known as monomethyl auristatin F and E (MMAF/E).[12,29] MMAE/F are equipotent, antimitotic cytotoxic drugs that are structurally derived from Dolastatin-10 and have shown to induce cell death through a G2/M cell cycle arrest following microtubule assembly disruption.[33−37] However, MMAE has been reported to have bystander effects upon antibody release via its capacity to passively diffuse from targeted tumor cells via cell membranes and to accumulate within nearby healthy cells, thereby causing serious side effects. Of note is that this phenomenon is not observed with the MMAF counterpart due to it having a charged C-terminal phenylalanine residue preventing cell membrane passive diffusion.[13,33−36,38−43]

Against this backdrop, we decided to extend our SNAP-tag-auristatin studies using the microtubulin poison, Auristatin F (AuriF), as the payload, and a linker prepared via a novel click coupling strategy to create an auristatin−linker−BG piece for SNAP-tag conjugation.[12,29] The field of linker type has been extensively reviewed, in which each class as cleavable versus noncleavable has advantages and disadvantages.[44−46] In our case, the expectation was to reduce off-target toxicity using a noncleavable linker containing a poly(ethylene glycol) (PEG) moiety for improving the pharmacokinetic and pharmacodynamic properties of the antibody fragment.[44−46] Here, ADC internalization through endocytosis linking either with recycling


https://doi.org/10.1021/acsomega.2c06844
ACS Omega 2023, 8, 4026−4037

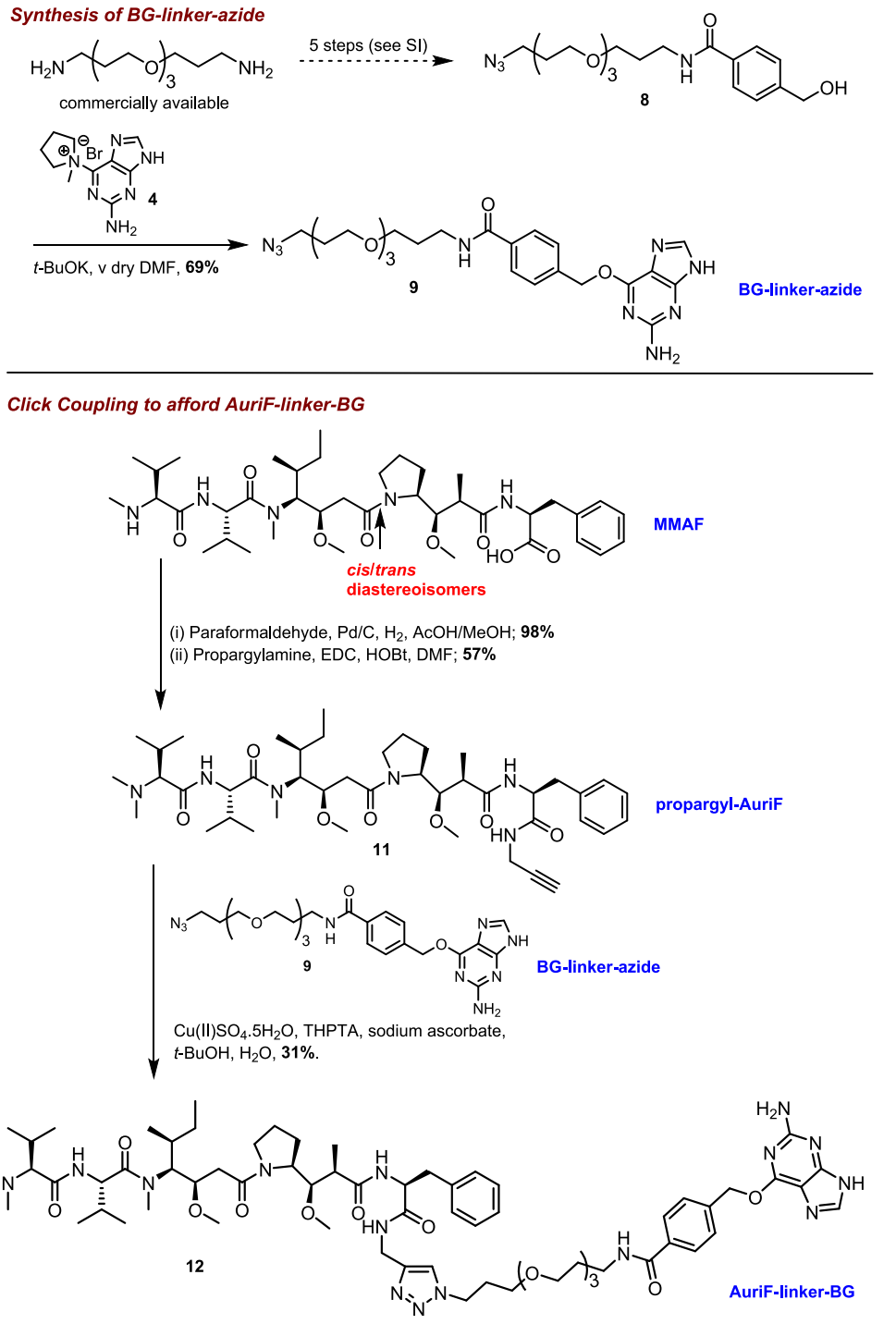


**Figure 2.** Synthesis of AuriF−linker−BG for SNAP-tag conjugation. An overview of the essential synthetic chemistry used in the construction of the AuriF−linker−BG precursor for SNAP-tag conjugation to the scFv. A full description of all steps is given in the Supporting Information.

of the ADC-receptor complex through transporters or with endo-lysosomal trafficking, followed by subsequent linker/antibody proteolysis, would lead to the delivery of the payload intracellularly. The structure of our ADC target as scFv−linker−AuriF is shown in Figure 1.

Based on these criteria, we have generated an AuriF-SNAP-tag immunoconjugate containing a noncleavable linker targeting EGFR-expressing tumor cells. The SNAP-tagged version of the recombinant anti-EGFR scFv1711 was derived from the FDA-approved human mAb panitumumab (with superior binding activity compared to its parental counterparts) and was conjugated to the synthetically derived BG-modified AuriF. The targeted toxicity of this ADC was then assessed *in vitro*, demonstrating the suitability of a novel click chemistry-based conjugation strategy for producing our promising recombinant ADC and paving the way for extension into a future broader study on linker type.

## RESULTS AND DISCUSSION

**Synthesis of AuriF−Linker−BG for SNAP-Tag Conjugation.** The chemical synthesis to produce the AuriF−linker−BG piece required for SNAP-tag conjugation is shown in



https://doi.org/10.1021/acsomega.2c06844
ACS Omega 2023, 8, 4026−4037

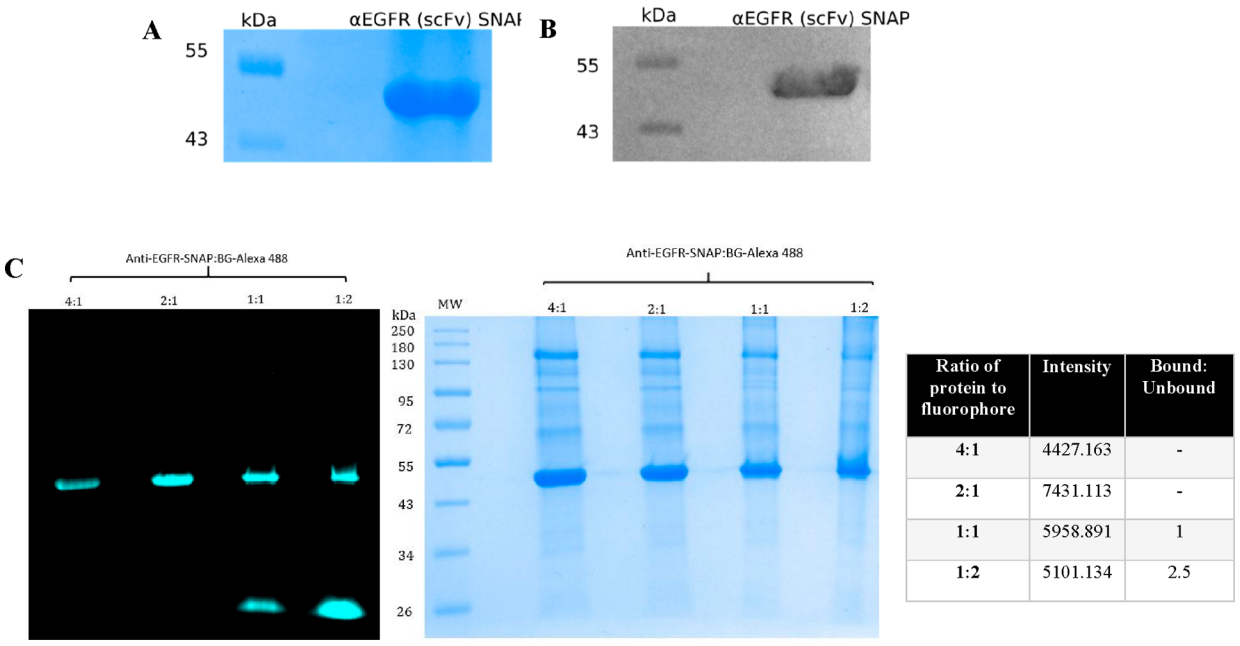


| Ratio of protein to fluorophore | Intensity | Bound: Unbound |
|---|---|---|
| 4:1 | 4427.163 | - |
| 2:1 | 7431.113 | - |
| 1:1 | 5958.891 | 1 |
| 1:2 | 5101.134 | 2.5 |

**Figure 3.** Protein validation/characterization of IMAC-purified 1711(scFv)-SNAP. (A) SDS-PAGE gel of purified and concentrated 1711(scFv)-SNAP. (B) 1711(scFv)-SNAP was subjected to a Western Blot analysis. A primary anti-his rabbit antibody (1:1000) was used, followed by a secondary goat anti-rabbit HRP antibody conjugate (1:5000). (C) Fluorescent blot and corresponding 10% SDS-PAGE gel of 1711(scFv)-SNAP conjugated with BG-Alexa Fluor 488 at different (protein: fluorophore) ratios 4:1, 2:1, 1:1 and 1:2.

Figure 2, in which the key step was convergent click coupling of BG−linker−azide (Supporting Information, Experimental Section, No. 9, Figures S19−S21) to propargyl-AuriF (Supporting Information, Experimental Section, No. 11, Figures S24 and S25) containing the auristatin C-terminus functionalized as its *N*-propargylamide. The BG−linker−azide could be prepared in six straightforward steps from a commercially available peg-diamine (4,7,10-trioxa-1,13-tridecanediamine) with a relatively short two-peg unit. Its length turned out to be suitable for successful SNAP-tag conjugation to take place (see the Biological Section). Yields for the six steps were good to excellent, although the final step introducing the BG group via $S_NAr$ coupling of the anion of the benzylic alcohol (Supporting Information, Experimental Section, No. 8, Figures S16−S18) required extremely dry dimethylformamide (DMF) to achieve a good yield.[47] Unlike the BG entities of other SNAP-tag cases, the phenyl group in our case was chosen to contain a carboxyl group (normally, this is a methylene group) *para* to the benzylic carbon for guanine attachment. This was selected to both facilitate coupling to the linker as well as assist with SNAP-tag substitution with the transferase thiolate due to the carboxyl group's electron-withdrawing effect.[12,28,29] Coupling of the BG−linker−azide (Supporting Information, Experimental Section, No. 9, Figures S19−S21) to propargyl-AuriF using standard click conditions and the click ligand tris-hydroxypropyltriazolylmethylamine (THPTA) gave the desired product in 31% yield after chromatography (on a 20 mg scale of Supporting Information, Experimental Section, No. 11, Figures S24 and S25). All new compounds in the sequence were satisfactorily and fully characterized by $^1$H and $^{13}$C NMR spectroscopy together with HRMS. In agreement with the literature, NMR spectra for the final AuriF−linker−BG (Supporting Information, Experimental Section, No. 12, Figures S26−S29) as the precursor for SNAP-tag coupling were complex due to the presence of *cis* and *trans* geometrical isomers around the tertiary amide of the pyrrolidine ring of AuriF.[47−49] Of these, only the elongated structure of the *trans* isomer fits into the tubulin receptor pocket between the $\alpha$ and $\beta$ units of the tubulin dimer. As a result, only the *trans* isomer is biologically active.[48] Hence, as a result of the NMR spectroscopic complexity of (Supporting Information, Experimental Section, No. 12, Figures S26−S29), we relied on TLC, HRMS, and the presence of a prominent benzylic methylene singlet at around 5.6 ppm in the $^1$H NMR spectrum for the BG methylene group as diagnostic signals (see the Supporting Information). Figure 2 summarizes the synthesis of both the BG−linker−azide (Supporting Information, Experimental Section, No. 9, Figures S19−S21) and the final AuriF−linker−BG (Supporting Information, Experimental Section, No. 12, Figures S26−S29) constructs.

***In Silico* Cloning, Expression, and Characterization of 1711(scFv)-SNAP.** The scFv-based SNAP-tag fusion protein 1711(scFv)-SNAP was transiently expressed in HEK293T cells. The recombinant protein was collected from the cell culture supernatant (CCSN) and purified using immobilized metal affinity chromatography (IMAC) by employing the C-terminal 6xHis-tag, yielding 5.87 mg of protein from 2.25L of CCSN, as determined by densitometric analysis. Purified 1711(scFv)-SNAP had an estimated purity of 38%, highlighting the need for a multistep purification process to cater for high quality (>90% purity) proteins en route to preclinical studies. The IMAC-purified fusion protein was then run on a 10% SDS-PAGE gel under denaturing conditions. Protein bands corresponding to the theoretical size of 1711(scFv)-SNAP (50.35 kDa) were observed between 48 and 55 kDa (Figure 3A). Thereafter, the separated fusion protein was transferred to a PVDF membrane for western blot analysis. Briefly, this membrane was successively exposed to a primary anti-his antibody, and a secondary HRP-conjugated antibody was used to confirm the presence of the putative protein by chemiluminescence. The detection of the N-terminal 6xHis-tag on the immunoblot (Figure 3B) confirmed


https://doi.org/10.1021/acsomega.2c06844
ACS Omega 2023, 8, 4026−4037

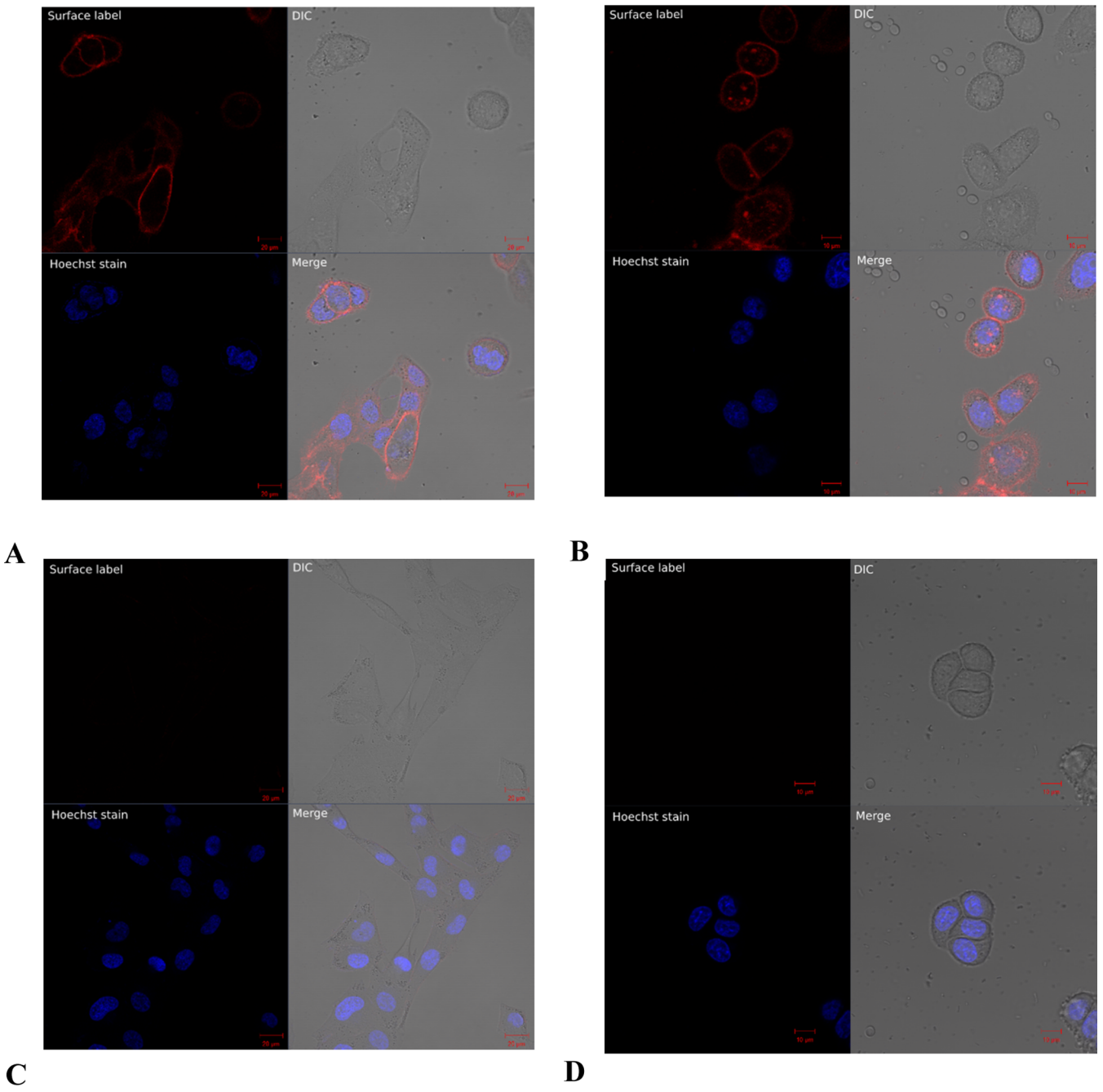


**Figure 4.** Live cell imaging of 1711(scFv)-SNAP-Alexa Fluor 647 binding to EGFR-positive cells. (A–D) Confocal microscopy images of 1711(scFv)-SNAP-Alexa Fluor 647 binding and uptake (red) in target cell lines after 30 min of incubation at room temperature. Hoechst was used as a stain for the nuclei (blue). (A) Surface binding of 1711(scFv)-SNAP-Alexa Fluor 647 to A431 cells at 37 °C. (B) Specific surface binding and internalization of 1711(scFv)-SNAP-Alexa Fluor 647 in MDA-MB-468 cells at room temperature. (C) No binding of 1711(scFv)-SNAP-Alexa Fluor 647 to the EGFR-negative A2058 cells. (D) Vehicle control with MDA-MB-468 cells incubated in 1× PBS at room temperature.

the identity and integrity of the recombinant SNAP-tag fusion protein. Numerous conjugation experiments were then performed with BG-modified fluorophores to validate the functionality of the SNAP-tag moiety of 1711(scFv)-SNAP. As such, BG-modified fluorophores are excellent indicators for further validating the presence of full-length protein while concurrently assessing the functionality of the SNAP-tag component. BG-Alexa Fluor 488 conjugation to 1711(scFv)-SNAP was set up in the following ratios (protein to fluorophore): 4:1, 2:1, 1:1, and 1:2 (Figure 3C). The 2:1 conjugation ratio generated the highest fluorescence intensity visually, confirming that this ratio was optimal for reaction with the BG-modified substrate. Of note, higher fluorescence intensity was not detected in the presence of other protein ratios (4:1 and 2:1).

**Binding Analysis of 1711(scFv)-SNAP on EGFR-Overexpressing Tumor Cells.** Live cell imaging was used to assess the binding activity of 1711(scFv)-SNAP-Alexa Fluor 647 (successful generation of 1711(scFv)-SNAP-Alexa 647 is confirmed by Figure 7A). After 30 min of incubation at room temperature, we observed specific surface binding of the SNAP-tag fusion protein to the EGFR-overexpressing cell lines A431



https://doi.org/10.1021/acsomega.2c06844
ACS Omega 2023, 8, 4026−4037

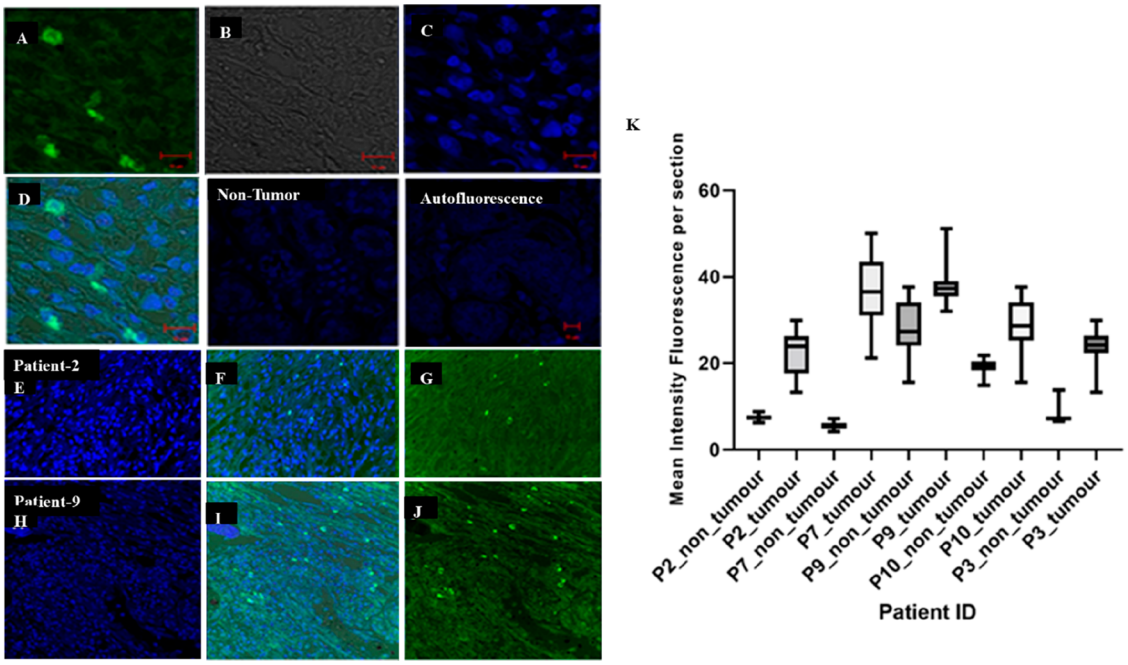


**Figure 5.** Binding of 1711(scFv)-SNAP on South African breast cancer patients' tissue sections and the pooled mean fluorescence intensities of EGFR expression. Using the LSM confocal 880 microscope, FFPE tissue sections were imaged. The mean of each patient's fluorescent intensity data was extracted and tabulated for comparison. (A) 1711(scFv)-SNAP conjugated to BG-Alexa488 labels the cell membrane. (B) The corresponding bright field panel displaying cell morphology. (C) The DAPI panel showing nuclear staining of cells. (D) Merged panel of A-C. The 1711(scFv)-SNAP pooled label data for patients, whereby patient means were compared using an ANOVA. The mean intensity data indicated significant differences between all tumour and non-tumour tissues in the selected patient samples. Qualitative differences are indicated as a comparison of the fluorescence image panels of patient 2 (E-G) and patient 9 (H-J). These samples were normalized against an autofluorescence control for each patient. Differences in mean fluorescent densities between tumour and non-tumour of selected patients 2, 3, 7, 9, and 10 (K).

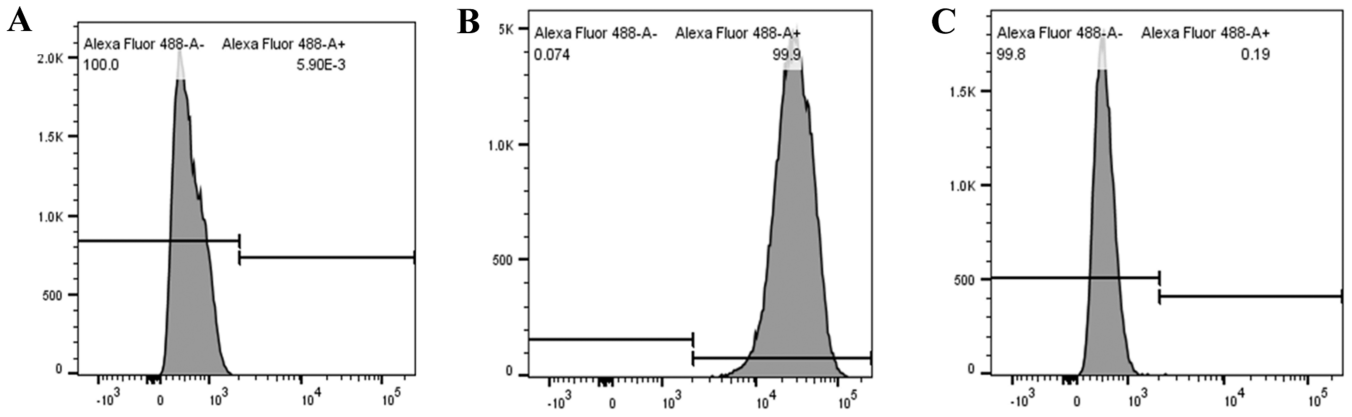


**Figure 6.** Flow cytometric analysis to determine the binding of Alexa 488-conjugated 1711(scFv)-SNAP to EGFR-positive cells. (A) Unstained cell populations. (B) Binding of BG-Alexa 488-labeled 1711(scFv)-SNAP fusion protein to EGFR-expressing MDA-MB-468 cells. (C) No binding of 1711(scFv)-SNAP-Alexa 488 fusion protein to EGFR-negative cells.

and MDA-MB-468 (Figure 4A,B) but no binding to the EGFR-negative A2058 (control) cells (Figure 4C). Additionally, there was no evidence of autofluorescence from the 1x PBS control, indicating that the observed signal was solely receptor-dependent (Figure 4D). Moreover, the binding potential of the antibody component of 1711(scFv)-SNAP was further validated by staining formalin-fixed paraffin-embedded (FFPE) breast cancer tissue sections of South African patients and deriving the pooled mean fluorescence intensities of EGFR expression from the images generated (Figure 5).

**Flow Cytometric Analysis of Receptor Density on EGFR-Overexpressing Tumor Cells.** As observed from Figure 6, there was complete binding (over 90% of the cell population was positive for EGFR) of the Alexa 488-labeled 1711(scFv)-SNAP to the EGFR-overexpressing MDA-MB-468 cells but not to the control cell line, A2058, denoting that the binding is receptor-dependent. The high specificity of saturation of the labeled fusion protein to discriminate overexpressed EGFR receptors from nonexpressing cells makes it an ideal tool for screening EGFR-positive cells preferentially from a multitude of cell populations.

**Conjugation of 1711(scFv)-SNAP to BG−Linker−AuriF for Cytotoxicity Studies.** After confirming the binding and internalization of 1711(scFv)-SNAP, the next step was to investigate the cytotoxic activity of the recombinant AuriF-based ADC. Therefore, the purified fusion protein was conjugated to


https://doi.org/10.1021/acsomega.2c06844
ACS Omega 2023, 8, 4026−4037

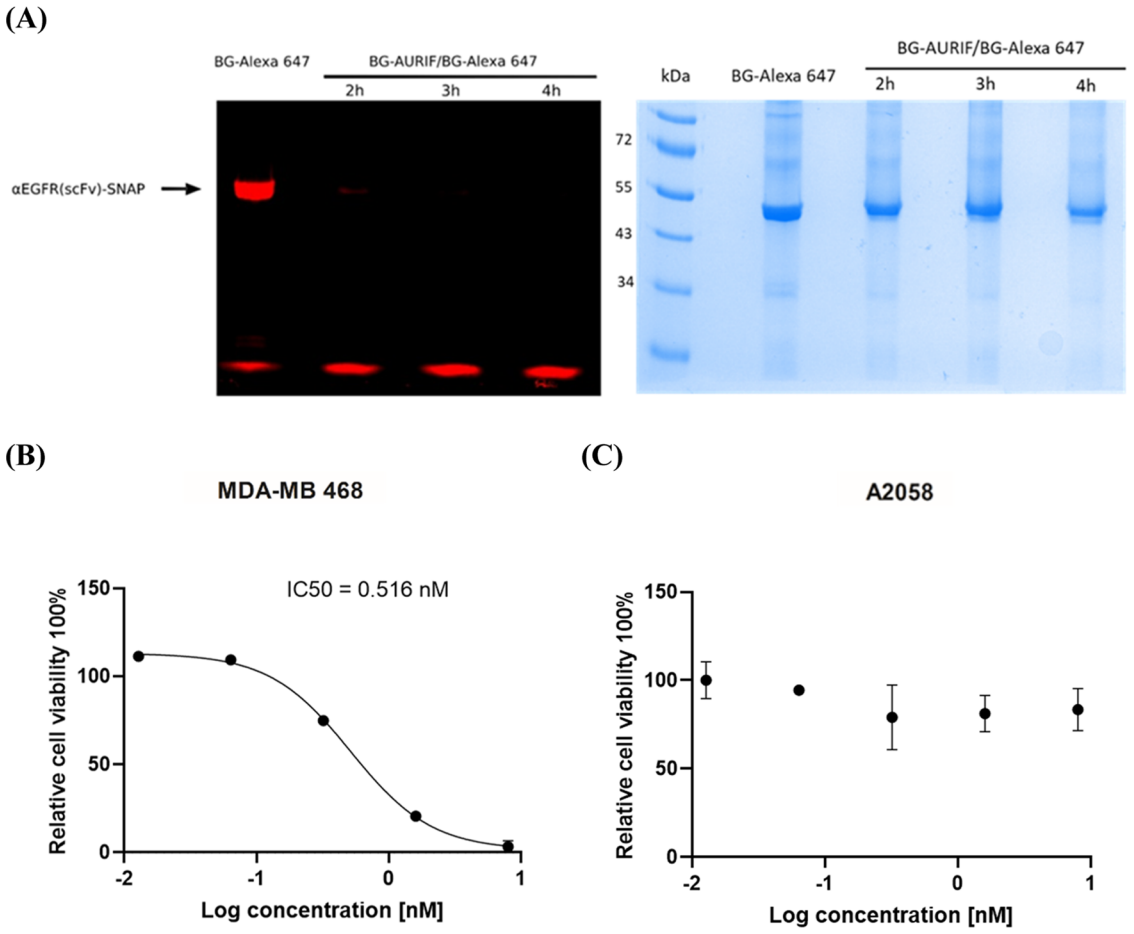


**Figure 7.** Cytotoxicity of 1711(scFv)-SNAP-AuriF toward EGFR-overexpressing tumor cells. (A) Fluorescent blot and associated 10% SDS-PAGE gel of 1711(scFv)-SNAP and 1711(scFv)-SNAP-AuriF (generated after 2, 3, and 4 h incubation) conjugated to BG-Alexa 647. (B, C) XTT viability assay was used to assess cytotoxicity following a 72 h incubation with 1711(scFv)-SNAP-AuriF on (B) MDA-MB-468 and (C) A2058 cells. $IC_{50}$ values relative to untreated cells were calculated using GraphPad Prism v5 software. Three biological repeats were made with duplicate treatments. Means and standard deviations are presented for each concentration.

BG−linker−AuriF in a 1:2 ratio. Thereafter, the conjugated fusion protein was post-incubated with BG-Alexa Fluor 647 to confirm the functionality of SNAP-tag and saturation of the SNAP-tag binding pocket with AuriF. Our findings show that a 3 h incubation with a 2-fold molar excess of BG−linker−AuriF is sufficient to saturate the fusion protein at room temperature (Figure 6A). After the removal of the unbound BG−linker−AuriF, the recombinant ADC was applied to MDA-MB-468 and A2058 cells in decreasing concentrations. The cellular proliferation rates were compared to those of vehicle-treated cells after 72 h of treatment (Figure 6B,C). The viability of the MDA-MB-468 cell lines was reduced (in a dose-dependent fashion) when incubated with 1711(scFv)-SNAP-AuriF, with an $IC_{50}$ value of 0.516 nM. The recombinant ADC had a negligible effect on the viability of the EGFR-negative (A2058) cell line (see Figure 7).

## CONCLUSIONS

ADCs represent clinically relevant therapeutic approaches aimed at minimizing off-target toxicities caused by conventional chemotherapies. Among the several existing antibody−drug conjugating strategies, modification of the N- or C-terminus by genetically encoding functional groups has proven to be a viable and most utilized option.[15−17] In this regard, the design and chemistry of linkers combining mAb to the payload have become an important component of ADC development.[50] Among several expected properties, the ability of the linker to self-immolate to release the payload, in addition to cleavage and ease-of-synthesis, forms the backbone of an effective and stable ADC.[51] Homogeneous ADC products such as ours are highly efficient in payload delivery, resulting in improved antitumour effects compared to heterogeneous ADC species.[52] These early-stage preclinical studies also confirm that stochastic labeling of mAbs with payloads inhibits smooth targeting of tumors by the generated ADC products, underscoring the need for a more precise approach in the development of ADCs with improved pharmacokinetic profiles.

Herein, we have demonstrated that a recombinant ADC generated by a novel click chemistry conjugation of a SNAP-tag-based scFv fusion protein to an antineoplastic payload, AuriF, by a synthetic chemical linker, is a potent ADC candidate for the therapy of EGFR-overexpressing tumor cells. The unique characteristics of our click chemistry-generated linker with a longer spacer allows for wider distancing between the scFv-SNAP component and AuriF, thereby limiting the possibility of unfavorable steric hindrance. Furthermore, this highly versatile linker provides options for coupling other synthetic payloads in place of AuriF. Taken together, our approach offers several advantages, including (1) site-selective labeling of the SNAP-tag moiety in the recombinant fusion protein (at the C-terminus) by


https://doi.org/10.1021/acsomega.2c06844
ACS Omega 2023, 8, 4026−4037

1:1 interaction with the BG-modified substrate, resulting in the generation of a homogeneous product (DAR of 1), (2) unlikelihood of the formation of antidrug antibodies due to the absence of non-native human protein (SNAP-tag is a modified version of a human-based enzyme) compared to others, and (3) a higher probability of improved tumor transduction due to relatively smaller scFv antibody format in comparison to previous studies.[18,19,21]

In addition, our study highlights the feasibility of generating a potent ADC with reduced reaction steps by leveraging click chemistry conjugation reactions. Here, we confirm that the conjugation reaction of a SNAP-tag-based recombinant fusion protein to a BG-modified antimitotic drug is achieved within 3 h in a reproducible way. The novel ADC exhibited EGFR receptor-specific binding and internalization of positive tumor cells but not to tumors lacking EGFR expression, resulting in the selective killing of the former.

In conclusion, subsequent *in vivo* evaluation of the novel click chemistry-generated ADC is imperative to showcase its actual properties as a potential clinically graded ADC candidate for the therapy of EGFR-positive tumors. Overall, the preliminary *in vitro* results obtained provide proof of principle for the suitability of this click chemistry approach in the generation of homogeneous and biologically active recombinant ADCs.

## EXPERIMENTAL PROCEDURES

**Cell Culture.** All cell culture reagents were purchased from Gibco by Life Technologies (Thermo Fisher Scientific, South Africa). Human embryonic kidney (HEK293T (ATCC: CRL-11268)) cells were cultured in Roswell Park Memorial Institute (RPMI)-1640 medium (containing 2 mM L-glutamine, 3.7 g/L $NaHCO_3$ and 15 mg/L phenol red and supplemented with 10% (v/v) fetal bovine serum (FBS) and 1% (v/v) 100 U/mL penicillin−streptomycin) at 37 °C with 95% humidity and 5% $CO_2$. MDA-MB-468 (ATCC: HTB-132), A431 (ATCC: CRL-259), and A2058 (ATCC: CRL-11147) cells were cultured in Dulbecco's modified Eagle's medium (DMEM) (containing 2 mM L-glutamine, 3.7 g/L $C_3H_3NaO_3$ and 16 mg/L phenol red) supplemented as above. The ZOE Fluorescent Cell Imager (Bio-Rad, CA) was used to visualize and check the confluency of the cells.

**Synthesis of AuriF−Linker−BG for SNAP-Tag Conjugation.** Commercial MMAF was obtained from BrightGene Bio-Medical Technology (China) and N-methylated to Auristatin F (AuriF), which was synthetically transformed into AuriF−linker−BG, **12**. The key step of the sequence involved click coupling of propargyl-AuriF, **11** (prepared from 1-ethyl-3-(3-dimethylaminopropyl) carbodiimide (EDC) coupling of propargylamine to AuriF), to a BG−linker−azide construct, **9**. Azide, **9**, was prepared in six routine steps from commercially available 4,7,10-trioxa-1,13-tridecanediamine (a full description of the chemistry is given in the Supporting Information).

**Cloning, Expression, and Purification of 1711(scFv)-SNAP.** The scFv gene sequence (scFv1711) targeting EGFR was extracted from US patent US6235883B1 and subsequently subjected to IgBLAST analysis to compare the extracted sequences against existing immunoglobulin germline variable region gene sequences. After confirming the presence of intact complementarity-determining regions (CDRs) and framework regions (FRs) of the scFv, the scFv variable heavy chain ($V_H$) was isolated and linked with the corresponding variable light chain ($V_L$) using our lab-specific linker sequence. Following the alignment of scFv1711 to its parental sequence (using the CLC genomic workbench v11 software), the scFv was inserted into our generic pCB-scFv-SNAP expression plasmid, between *Sfi*I and *Not*I restriction sites. These unique restriction sites enabled generation of the pCB-scFv1711-SNAP expression plasmid via standard molecular cloning techniques.

Following transfection of the recombinant plasmid, the 1711(scFv)-SNAP-expressing HEK293T cells were grown in T175 culture flasks and were subjected to Zeocin selection (100 $\mu$g/mL) once 80−100% confluent. Protein expression was monitored by the level of expression of enhanced green fluorescent protein (eGFP). Cell culture supernatant was harvested every 3−4 days for a period of ±6 months or until sufficient protein was obtained (>1 mg/mL). The ÄKTA Avant system (GE Healthcare), which employs immobilized metal affinity chromatography (IMAC), was used to purify the recombinant 6x histidine-tagged fusion protein from the cell culture supernatant. Thereafter, the protein-containing fractions were pooled and concentrated using 10 kDa Amicon Ultra-15 centrifugal filter units (Sigma-Aldrich, South Africa) at 4225*g* (rpm) for 30 min. To remove salts and traces of imidazole, buffer exchange was carried out by centrifuging the concentrated sample with 1x phosphate-buffered saline (PBS) (pH 7.4) at 4255*g* for 30 min.

**Protein Characterization Using SDS-PAGE and Western Blotting.** Sodium dodecyl sulfate-polyacrylamide gel electrophoresis (SDS-PAGE) was used to separate the purified fusion protein (based on its molecular weight) under reducing conditions. The theoretical molecular weight of 1711(scFv)-SNAP (50.4 kDa) was calculated using the conversion calculator available at https://www.aatbio.com/tools/calculate-peptide-and-protein-molecular-weight-mw. Purified protein was denatured at 95 °C for 10 min and mixed with 4× Laemmli protein sample buffer (Bio-Rad). The protein sample was then loaded onto a 10% SDS-PAGE gel and run at 100 V for 20 min, followed by 150 V for 70 min on the Mini-PROTEAN Tetra Cell system (Bio-Rad). Next, the gel was stained with Aqua staining solution (Vacutec, South Africa), following the manufacturer's instructions, to allow for the visualization of the protein bands. The Gel Doc XR+ (Gel Doc XR System, Bio-Rad) was used for image capture. Additionally, western blot analysis was used to further validate the integrity of the purified 1711(scFv)-SNAP. Protein bands were transferred from an unstained SDS-PAGE gel to a PVDF membrane (25V, 10 min) using the Bio-Rad Trans-Blot Turbo system. The PVDF membrane was blocked in Super-Block (PBS) Blocking Buffer (Thermo Fisher Scientific, South Africa) for 1 h. The membrane was then incubated overnight with primary anti-his rabbit antibody (1:1000) (Qiagen, Germany) at room temperature, followed by a 1 h incubation with secondary Goat anti-Rabbit horseradish peroxidase (HRP) antibody conjugate (1:5000) (Bio-Rad) at room temperature. For the detection of the secondary antibody substrate, the membrane was incubated in 4 mL of TMB Blotting Solution for 1 min and then rinsed in $dH_2O$ to stop the reaction. The Gel Doc XR+ (Gel Doc XR System, Bio-Rad) was used for image capture.

**Conjugation of 1711(scFv)-SNAP to BG-Modified Substrates.** *Conjugation to BG-Alexa Fluor 488/647.* Conjugation reactions with BG derivatives were carried out to confirm the functionality of the enzymatic SNAP-tag element of the 1711(scFv)-SNAP fusion protein. Commercially available BG-modified fluorophores, SNAP-Surface BG-Alexa Fluor 488 (BG-Alexa 488), and SNAP-Surface BG-Alexa Fluor 647 (BG-Alexa 647), purchased from New England Biolabs are


https://doi.org/10.1021/acsomega.2c06844
ACS Omega 2023, 8, 4026−4037

photostable fluorescent substrates used to label SNAP-tag fusion proteins in solution or in live cells. The conjugation reaction (1:1 ratio of protein to fluorophore) was set up as follows: 1 mM dithiothreitol, 5 $\mu$M BG-Alexa 488/647 and 5 $\mu$M 1711(scFv)-SNAP, in 1× PBS (pH 7.4) at a final volume of 15 $\mu$L. After incubation in dark conditions at 37 °C for 1 h, the reaction mixture was run on a 10% SDS-PAGE gel, and the iBright FL1500 Imaging System (Invitrogen, Thermo Fisher Scientific, South Africa) was used for visualization of the fluorescent signal.

*Conjugation to BG−Linker−AuriF.* The labeling of 1711-(scFv)-SNAP to BG−linker−AuriF was prepared in a 1:2 ratio, with 1 mM Dithiothreitol, 20 $\mu$M BG−linker−AuriF, 10 $\mu$M 1711(scFv)-SNAP, buffered in 1× PBS (pH 7.4) to a final volume of 1 mL. The conjugation reaction was incubated at room temperature for 2, 3, and 4 h. To confirm the saturation of SNAP-tag with BG−linker−AuriF, a subsequent conjugation was carried out with BG-Alexa 647, and the resulting mixture was run on a 10% SDS-PAGE gel. Thus, after confirming the optimal time that would allow saturation of the SNAP-tag binding pocket with BG−linker−AuriF, conjugation to BG−linker−AuriF was repeated, and traces of the unconjugated BG-modified drug were removed using 10 kDa Amicon Ultra-15 centrifugal filter units (Sigma-Aldrich, South Africa) according to the manufacturer's instructions. The reaction mixture was filter-sterilized using a 0.22 $\mu$m syringe filter (Biosmart, South Africa) prior to use.

**Analysis of Surface Binding via Confocal Microscopy.** For each treatment, $2 \times 10^4$ of A431, MDA-MB-468, and A2058 cells were seeded in live cell viewing dishes and incubated for 48 h at 37 °C in a 5% $CO_2$ incubator with 95% humidity. 1711(scFv)-SNAP was conjugated in a 1:1 ratio with BG-Alexa 647 at 37 °C for 1 h in the dark. Following this, the conjugated reaction mixture was centrifuged to remove any unconjugated fluorophore using Zeba Spin desalting columns (Thermo Fisher Scientific, South Africa) at 1500*g*. The mixture was filtered using sterilized 0.22 $\mu$m filters and stored at −20 °C overnight. The conjugation reaction was diluted in a 1:1 ratio of 1711(scFv)-SNAP-BG-Alexa 647 to unsupplemented DMEM. For the positive treatment and negative controls, cells were incubated at room temperature with diluted 1711(scFv)-SNAP-BG-Alexa 647 and 1× PBS (pH 7.4), respectively, for 20 min. After treatment, the labeling media was decanted, followed by washing steps with unsupplemented DMEM media. Hoechst stain (1 ng/mL) was added, and the cells were incubated for a further 10 min at room temperature, followed by washing with unsupplemented DMEM.

Formalin-fixed, paraffin-embedded tissue sections of South African triple-negative breast cancer patients (HREC Ref: 564/2018) were rinsed in deionized water and dab-dried, and a ImmEdge Pen (H-4000, Vector Laboratories, Peterborough, U.K.) was used to "ring the island" around the section to create an area onto which 100−200 $\mu$L of labeled SNAP-tag was pipetted (to the full volume of the labeled 15 $\mu$g of SNAP-tag) with added Hoechst 33342 counterstain. This was incubated for 1 h in the dark at room temperature. The section was then washed 3× using PBS and incubated with 0.1% Sudan Black for 10 min and then rinsed with PBST and then double distilled $H_2O$ and mounted in an aqueous solution for viewing.

Thereafter, the cells/tissue sections were viewed at the Confocal and Light Microscope Imaging Facility (University of Cape Town, South Africa), and images were captured on the Zeiss confocal scanner microscope (LSM880) with Airyscan. All experiments were performed in triplicate.

**Flow Cytometric Analysis for Determination of EGFR Receptor Expression Density.** To determine the binding activity of 1711(scFv)-SNAP fusion protein, flow cytometry analysis was carried out using fusion proteins labeled with BG-Alexa 488. Briefly, BG-Alexa Fluor 488 was incubated with 1711(scFv)-SNAP (in a 1:1 ratio) in the presence of 1 mM DTT in 1× PBS (pH 7.4) at 37 °C for 1 h. Afterward, any unconjugated fluorophore was removed by size exclusion chromatography using 40K Zeba Spin desalting columns (Thermo Fisher Scientific, South Africa) at 13 000*g* for 1 min. Eluted fusion proteins were then used to label target (MDA-MB-468) and control (A2058) cell lines.

Cells were cultured in DMEM media supplemented with 10% (v/v) FBS and 1% (v/v) 100 U/mL penicillin−streptomycin antibiotics cocktail until the desired confluency was reached and were lifted using 1× Trypsin/EDTA solution (Life Technologies Corporation, Biocompare). Next, $5 \times 10^5$ live cells were washed and aliquoted into FACS tube and centrifuged at 500*g* for 5 min at 4 °C. Thereafter, cell pellets were resuspended and washed in 1 mL of 1× PBS. After 2× washing steps, cells were stained with 500 $\mu$L (1 $\mu$L in 1 mL of 1× PBS) of live/dead Alexa Fluor 405 stain (Thermo Fisher Scientific) in the dark and incubated on ice for 30 min. Next, cells were resuspended in 1× FASC buffer, washed with 1× PBS, and then stained with labeled fusion protein on ice for 1 h. Labeled cells were then fixed in 4% (v/v) paraformaldehyde (PFA), incubated at room temperature in the dark for 15 min, and resuspended in 200 $\mu$L of 1× PBS for data acquisition at the Flow Cytometry Core Facility, IDM (University of Cape Town, South Africa). The results obtained were then analyzed on Flow Jo software v10.8.1 (BD Biosciences).

***In Vitro* Cytotoxicity Studies.** MDA-MB-468 and A2058 tumor cell lines were seeded in a 96-well plate, with $5 \times 10^3$ cells in 100 $\mu$L of media plated per well. Cells were cultured in DMEM media (supplemented with 10% (v/v) FBS and 1% (v/v) 100 U/mL penicillin−streptomycin) and incubated at 37 °C in a 95% humidity and 5% $CO_2$ atmosphere. After 24 h, cells were treated with a range of 1711(scFv)-SNAP-AuriF concentrations (1000 to 0.013 nM in a final volume of 200 $\mu$L). After 68 h of incubation with the recombinant ADC, XTT and *N*-methyl dibenzopyrazine methyl sulfate (Roche, Germany) were mixed in a 50:1 ratio, and 51 $\mu$L of the mixture was added per well and incubated for 4 h. The conversion of the XTT reagent to the substrate was measured by spectrophotometry using the iMark Microplate Reader (Bio-Rad) and determined as the difference of $OD_{450\,nm}$ and $OD_{655\,nm}$. The absorbance readings were analyzed using GraphPad Prism v5 software to determine the 50% inhibitory concentration ($IC_{50}$ value) of 1711(scFv)-SNAP-AuriF on the respective tumor cell lines. Experiments were performed thrice with two technical repeats.

## ■ ASSOCIATED CONTENT

### Supporting Information

The Supporting Information is available free of charge at https://pubs.acs.org/doi/10.1021/acsomega.2c06844.

Additional information for the various steps involved in the synthesis of BG−linker−AuriF; materials and methods; scheme for synthesis; $^1$H NMR and $^{13}$C NMR spectra; mass spectra; and relevant references (PDF)



https://doi.org/10.1021/acsomega.2c06844
ACS Omega 2023, 8, 4026−4037

## AUTHOR INFORMATION


### Corresponding Authors

**Roger Hunter** − *Department of Chemistry, University of Cape Town, Cape Town 7700, South Africa;* orcid.org/0000-0001-8775-083X; Phone: +27-21-650-2544; Email: roger.hunter@uct.ac.za

**Stefan Barth** − *Medical Biotechnology and Immunotherapy Research Unit, Institute of Infectious Disease and Molecular Medicine, Faculty of Health Sciences and South African Research Chair in Cancer Biotechnology, Department of Integrative Biomedical Sciences, Faculty of Health Sciences, University of Cape Town, Cape Town 7700, South Africa;* orcid.org/0000-0001-9589-653X; Phone: +27-21-406-6938; Email: stefan.barth@uct.ac.za

### Authors

**Allan M. Huysamen** − *Department of Chemistry, University of Cape Town, Cape Town 7700, South Africa;* orcid.org/0000-0003-3170-0555

**Olaolu E. Fadeyi** − *Department of Chemistry, University of Cape Town, Cape Town 7700, South Africa*

**Grace Mayuni** − *Medical Biotechnology and Immunotherapy Research Unit, Institute of Infectious Disease and Molecular Medicine, Faculty of Health Sciences, University of Cape Town, Cape Town 7700, South Africa*

**Dennis M. Dogbey** − *Medical Biotechnology and Immunotherapy Research Unit, Institute of Infectious Disease and Molecular Medicine, Faculty of Health Sciences, University of Cape Town, Cape Town 7700, South Africa*

**Neelakshi Mungra** − *Medical Biotechnology and Immunotherapy Research Unit, Institute of Infectious Disease and Molecular Medicine, Faculty of Health Sciences, University of Cape Town, Cape Town 7700, South Africa; Centre for Immunity and Immunotherapies, Seattle Children's Research Institute, Seattle, Washington 98101, United States;* orcid.org/0000-0002-5993-3943

**Fleury A. N. Biteghe** − *Department of Radiation Oncology and Biomedical Sciences, Cedars-Sinai Medical, Los Angeles, California 90048, United States*

**Natasha Hardcastle** − *Medical Biotechnology and Immunotherapy Research Unit, Institute of Infectious Disease and Molecular Medicine, Faculty of Health Sciences, University of Cape Town, Cape Town 7700, South Africa*

**Dharanidharan Ramamurthy** − *Medical Biotechnology and Immunotherapy Research Unit, Institute of Infectious Disease and Molecular Medicine, Faculty of Health Sciences, University of Cape Town, Cape Town 7700, South Africa*

**Olusiji A. Akinrinmade** − *Medical Biotechnology and Immunotherapy Research Unit, Institute of Infectious Disease and Molecular Medicine, Faculty of Health Sciences, University of Cape Town, Cape Town 7700, South Africa; Department of Molecular Pharmacology, Albert Einstein College of Medicine, Bronx, New York 10461, United States*

**Krupa Naran** − *Medical Biotechnology and Immunotherapy Research Unit, Institute of Infectious Disease and Molecular Medicine, Faculty of Health Sciences, University of Cape Town, Cape Town 7700, South Africa*

**Susan Cooper** − *Division of Physiological Sciences, Department of Human Biology, University of Cape Town, Cape Town 7700, South Africa*

**Dirk Lang** − *Division of Physiological Sciences, Department of Human Biology, University of Cape Town, Cape Town 7700, South Africa*

**Wolfgang Richter** − *TUBE Pharmaceuticals, 1110 Wien, Austria*

Complete contact information is available at: https://pubs.acs.org/10.1021/acsomega.2c06844

### Author Contributions

◆S.B. and R.H. contributed equally to this work.



### Funding

This work is based on the research supported by the South African Research Chairs Initiative of the Department of Science and Technology (DST) and the National Research Foundation (NRF) of South Africa. The NRF and the South African Research Chair in Cancer Biotechnology have provided bursaries to support students contributing to this work. Research reported in this publication was also partially supported by the Strategic Health Innovation Partnerships (SHIP) Unit of the South African Medical Research Council with funds received from the South African Department of Science and Technology.


### Notes

The authors declare no competing financial interest.

## ACKNOWLEDGMENTS


The authors thank the IDM Flow Cytometry Core Facility (UCT), the Confocal and Light Microscope Imaging Facility (UCT), as well as the Department of Chemistry (UCT) for the assistance provided in the form of infrastructure and technical support.


## REFERENCES


(1) Biteghe, F. A. N.; Mungra, N.; Chalomie, N. E.; Ndong, J. D.; Engohang-Ndong, J.; Vignaux, G.; Padayachee, E.; Naran, K.; Barth, S. Advances in epidermal growth factor receptor specific immunotherapy: Lessons to be learned from armed antibodies. *Oncotarget* **2020**, *11*, 3531.

(2) Guerrab, A. E.; Bamdad, M.; Kwiatkowski, F.; Bignon, Y. J.; Penault-Llorca, F.; Aubel, C. Anti-EGFR monoclonal antibodies and EGFR tyrosine kinase inhibitors as combination therapy for triple-negative breast cancer. *Oncotarget* **2016**, *7*, 73618.

(3) Gurdal, H.; Tuglu, M. M.; Bostanabad, S. Y.; Dalkiliç, B. Partial agonistic effect of cetuximab on epidermal growth factor receptor and Src kinase activation in triple-negative breast cancer cell lines. *Int. J. Oncol.* **2019**, *54*, 1345−1356.

(4) Giusti, R. M.; Shastri, K. A.; Cohen, M. H.; Keegan, P.; Pazdur, R. FDA drug approval summary: Panitumumab (Vectibix). *Oncologist* **2007**, *12*, 577−583.

(5) Goldberg, R. M.; Kirkpatrick, P. Cetuximab. *Nat. Rev. Drug Discovery* **2005**, *4*, S10−S11.

(6) Cohen, M. H.; Chen, H.; Shord, S.; Fuchs, C.; He, K.; Zhao, H.; Sickafuse, S.; Keegan, P.; Pazdur, R. Approval Summary: Cetuximab in Combination With Cisplatin or Carboplatin and 5-Fluorouracil for the First-Line Treatment of Patients With Recurrent Locoregional or Metastatic Squamous Cell Head and Neck Cancer. *Oncologist* **2013**, *18*, 460−466.

(7) Kazandjian, D.; Blumenthal, G. M.; Yuan, W.; He, K.; Keegan, P.; Pazdur, R. FDA approval of gefitinib for the treatment of patients with metastatic EGFR mutation−positive non−small cell lung cancer. *Clin. Cancer Res.* **2016**, *22*, 1307−1312.

(8) Cohen, M. H.; Johnson, J. R.; Chen, Y. F.; Sridhara, R.; Pazdur, R. FDA drug approval summary: erlotinib (Tarceva) tablets. *Oncologist* **2005**, *10*, 461−466.

(9) Criscitiello, C.; Morganti, S.; Curigliano, G. Antibody−drug conjugates in solid tumors: a look into novel targets. *J. Hematol. Oncol.* **2021**, *14*, No. 20.

(10) Madheswaran, S.; Mungra, N.; Biteghe, F. A.; De la Croix Ndong, J.; Arowolo, A. T.; Adeola, H. A.; Ramamurthy, D.; Naran, K.;

Khumalo, N. P.; Barth, S. Antibody-Based Targeted Interventions for the Diagnosis and Treatment of Skin Cancers. *Anti-Cancer Agents Med. Chem.* **2021**, *21*, 162−186.
(11) Kobayashi, H.; Griffiths, G. L.; Choyke, P. L. Near-infrared photoimmunotherapy: Photoactivatable antibody−drug conjugates (ADCs). *Bioconjugate Chem.* **2020**, *31*, 28−36.
(12) Woitok, M.; Klose, D.; Di Fiore, S.; Richter, W.; Stein, C.; Gresch, G.; Grieger, E.; Barth, S.; Fischer, R.; Kolberg, K.; Niesen, J. Comparison of a mouse and a novel human scFv-SNAP-auristatin F drug conjugate with potent activity against EGFR-overexpressing human solid tumor cells. *OncoTargets Ther.* **2017**, *10*, 3313.
(13) Smith, L. M.; Nesterova, A.; Alley, S. C.; Torgov, M. Y.; Carter, P. J. Potent cytotoxicity of an auristatin-containing antibody-drug conjugate targeting melanoma cells expressing melanotransferrin/p97. *Mol. Cancer Ther.* **2006**, *5*, 1474−1482.
(14) Hsu, M. A.; Okamura, S. M.; De Magalhaes Filho, C. D.; Bergeron, D. M.; Rodriguez, A.; West, M.; Yadav, D.; Heim, R.; Fong, J. J.; Garcia-Guzman, M. Cancer-targeted photoimmunotherapy induces antitumor immunity and can be augmented by anti-PD-1 therapy for durable anticancer responses in an immunologically active murine tumor model. *Cancer Immunol., Immunother.* **2022**, *72*, 151−168.
(15) Tang, H.; Liu, Y.; Yu, Z.; Sun, M.; Lin, L.; Liu, W.; Han, Q.; Wei, M.; Jin, Y. The analysis of key factors related to adcs structural design. *Front. Pharmacol.* **2019**, *10*, 373.
(16) Khongorzul, P.; Ling, C. J.; Khan, F. U.; Ihsan, A. U.; Zhang, J. Antibody−Drug Conjugates: A Comprehensive ReviewAntibody−Drug Conjugates in Cancer Immunotherapy. *Mol. Cancer Res.* **2020**, *18*, 3−19.
(17) Ponziani, S.; Di Vittorio, G.; Pitari, G.; Cimini, A. M.; Ardini, M.; Gentile, R.; Iacobelli, S.; Sala, G.; Capone, E.; Flavell, D. J.; Ippoliti, R.; Giansanti, F. Antibody-drug conjugates: the new frontier of chemotherapy. *Int. J. Mol. Sci.* **2020**, *21*, 5510.
(18) Mckertish, C. M.; Kayser, V. Advances and limitations of antibody drug conjugates for cancer. *Biomedicines.* **2021**, *9*, 872.
(19) Deonarain, M. P.; Xue, Q. Tackling solid tumour therapy with small-format drug conjugates. *Antibody Ther.* **2020**, *3*, 237−245.
(20) Hussain, A.; Amoury, M.; Barth, S. SNAP-tag technology: a powerful tool for site specific conjugation of therapeutic and imaging agents. *Curr. Pharm. Des.* **2013**, *19*, 5437−5442.
(21) Zhang, H.; Wang, Y.; Wu, Y.; Jiang, X.; Tao, Y.; Yao, Y.; Peng, Y.; Chen, X.; Fu, Y.; Yu, L.; et al. Therapeutic potential of an anti-HER2 single chain antibody−DM1 conjugates for the treatment of HER2-positive cancer. *Signal Transduction Targeted Ther.* **2017**, *2*, No. 17015.
(22) Deonarain, M. P.; Yahioglu, G.; Stamati, I.; Pomowski, A.; Clarke, J.; Edwards, B. M.; Diez-Posada, S.; Stewart, A. C. Small-format drug conjugates: a viable alternative to ADCs for solid tumours? *Antibodies* **2018**, *7*, 16.
(23) Aubrey, N.; Allard-Vannier, E.; Martin, C.; Bryden, F.; Letast, S.; Colas, C.; Lakhrif, Z.; Collinet, N.; Dimier-Poisson, I.; et al. Site-specific conjugation of auristatins onto engineered scFv using second generation maleimide to target HER2-positive breast cancer in vitro. *Bioconjugate Chem.* **2018**, *29*, 3516−3521.
(24) Yap, M. L.; McFadyen, J. D.; Wang, X.; Ziegler, M.; Chen, Y. C.; Willcox, A.; Nowell, C. J.; Scott, A. M.; Sloan, E. K.; Hogarth, P. M.; et al. Activated platelets in the tumor microenvironment for targeting of antibody-drug conjugates to tumors and metastases. *Theranostics* **2019**, *9*, 1154.
(25) Richards, D. A. Exploring alternative antibody scaffolds: Antibody fragments and antibody mimics for targeted drug delivery. *Drug Discovery Today: Technol.* **2018**, *30*, 35−46.
(26) Chen, L.; Liu, Y. H.; Li, Y. H.; Jiang, Y.; Xie, P. L.; Zhou, G. H.; Li, G. C. Anti-hepatoma human single-chain Fv antibody and adriamycin conjugates with potent antitumor activity. *Int. Immunopharmacol.* **2014**, *18*, 20−26.
(27) Walsh, S. J.; Bargh, J. D.; Dannheim, F. M.; Hanby, A. R.; Seki, H.; Counsell, A. J.; Ou, X.; Fowler, E.; Ashman, N.; Takada, Y.; et al. Site-selective modification strategies in antibody−drug conjugates. *Chem. Soc. Rev.* **2021**, *50*, 1305−1353.
(28) Bauerschlag, D.; Meinhold-Heerlein, I.; Maass, N.; Bleilevens, A.; Bräutigam, K.; Al Rawashdeh, W. E.; Di Fiore, S.; Haugg, A. M.; Gremse, F.; Steitz, J.; Fischer, R.; et al. Detection and specific elimination of EGFR+ ovarian cancer cells using a near infrared photoimmunotheranostic approach. *Pharm. Res.* **2017**, *34*, 696−703.
(29) Woitok, M.; Klose, D.; Niesen, J.; Richter, W.; Abbas, M.; Stein, C.; Fendel, R.; Bialon, M.; Püttmann, C.; Fischer, R.; Barth, S.; Kolberg, K. The efficient elimination of solid tumor cells by EGFR-specific and HER2-specific scFv-SNAP fusion proteins conjugated to benzylguanine-modified auristatin F. *Cancer Lett.* **2016**, *381*, 323−330.
(30) Merten, H.; Brandl, F.; Plückthun, A.; Zangemeister-Wittke, U. Antibody−Drug Conjugates for Tumor Targeting— Novel Conjugation Chemistries and the Promise of non-IgG Binding Proteins. *Bioconjugate Chem.* **2015**, *26*, 2176−2185.
(31) Chio, T. I.; Bane, S. L. Click Chemistry Conjugations. In *Antibody−Drug Conjugates*; Humana Press: New York, NY, 2020; pp 83−97.
(32) Vatansever, E. C.; Kang, J.; Tuley, A.; Ward, E. S.; Liu, W. R. An optimal "Click" formulation strategy for antibody-drug conjugate synthesis. *Bioorg. Med. Chem.* **2020**, *28*, No. 115808.
(33) Bouchard, H.; Viskov, C.; Garcia-Echeverria, C. Antibody−drug conjugates—a new wave of cancer drugs. *Bioorg. Med. Chem. Lett.* **2014**, *24*, 5357−5363.
(34) Kim, E. G.; Kim, K. M. Strategies and advancement in antibody-drug conjugate optimization for targeted cancer therapeutics. *Biomol. Ther.* **2015**, *23*, 493.
(35) Li, H.; Yu, C.; Jiang, J.; Huang, C.; Yao, X.; Xu, Q.; Yu, F.; Lou, L.; Fang, J. An anti-HER2 antibody conjugated with monomethyl auristatin E is highly effective in HER2-positive human gastric cancer. *Cancer Biol. Ther.* **2016**, *17*, 346−354.
(36) Sommer, A.; Kopitz, C.; Schatz, C. A.; Nising, C. F.; Mahlert, C.; Lerchen, H. G.; Stelte-Ludwig, B.; Hammer, S.; Greven, S.; Schuhmacher, J.; Braun, M. Preclinical Efficacy of the Auristatin-Based Antibody−Drug Conjugate BAY 1187982 for the Treatment of FGFR2-Positive Solid TumorsFGFR2-Targeting Antibody−Drug Conjugate in Cancer. *Cancer Res.* **2016**, *76*, 6331−6339.
(37) Bai, R.; Pettit, G. R.; Hamel, E. Structure-activity studies with chiral isomers and with segments of the antimitotic marine peptide dolastatin 10. *Biochem. Pharmacol.* **1990**, *40*, 1859−1864.
(38) Shefet-Carasso, L.; Benhar, I. Antibody-targeted drugs and drug resistance—challenges and solutions. *Drug Resist. Updates* **2015**, *18*, 36−46.
(39) Polson, A. G.; Calemine-Fenaux, J.; Chan, P.; Chang, W.; Christensen, E.; Clark, S.; de Sauvage, F. J.; Eaton, D.; Elkins, K.; Elliott, J. M.; Frantz, G.; et al. Antibody-drug conjugates for the treatment of non−hodgkin's lymphoma: target and linker-drug selection. *Cancer Res.* **2009**, *69*, 2358−2364.
(40) Ansell, S. M. Brentuximab vedotin. *Blood* **2014**, *124*, 3197−3200.
(41) Doronina, S. O.; Toki, B. E.; Torgov, M. Y.; Mendelsohn, B. A.; Cerveny, C. G.; Chace, D. F.; DeBlanc, R. L.; Gearing, R. P.; Bovee, T. D.; Siegall, C. B.; Francisco, J. A.; et al. Development of potent monoclonal antibody auristatin conjugates for cancer therapy. *Nat. Biotechnol.* **2003**, *21*, 778−784.
(42) Doronina, S. O.; Mendelsohn, B. A.; Bovee, T. D.; Cerveny, C. G.; Alley, S. C.; Meyer, D. L.; Oflazoglu, E.; Toki, B. E.; Sanderson, R. J.; Zabinski, R. F.; Wahl, A. F.; Senter, P. D. Enhanced activity of monomethylauristatin F through monoclonal antibody delivery: effects of linker technology on efficacy and toxicity. *Bioconjugate Chem.* **2006**, *17*, 114−124.
(43) Li, F.; Emmerton, K. K.; Jonas, M.; Zhang, X.; Miyamoto, J. B.; Setter, J. R.; Nicholas, N. D.; Okeley, N. M.; Lyon, R. P.; Benjamin, D. R.; Law, C. L. Intracellular Released Payload Influences Potency and Bystander-Killing Effects of Antibody-Drug Conjugates in Preclinical ModelsReleased Payload Impacts ADC Activity and Bystander Killing. *Cancer Res.* **2016**, *76*, 2710−2719.
(44) Kholodenko, I. V.; Kalinovsky, D. V.; Svirshchevskaya, E. V.; Doronin, I. I.; Konovalova, M. V.; Kibardin, A. V.; Shamanskaya, T. V.; Larin, S. S.; Deyev, S. M.; Kholodenko, R. V. Multimerization through


https://doi.org/10.1021/acsomega.2c06844
*ACS Omega* 2023, 8, 4026−4037

pegylation improves pharmacokinetic properties of scFv fragments of GD2-specific antibodies. *Molecules* **2019**, *24*, 3835.
(45) Bargh, J. D.; Isidro-Llobet, A.; Parker, J. S.; Spring, D. R. Cleavable linkers in antibody−drug conjugates. *Chem. Soc. Rev.* **2019**, *48*, 4361−4374.
(46) Su, Z.; Xiao, D.; Xie, F.; Liu, L.; Wang, Y.; Fan, S.; Zhou, X.; Li, S. Antibody−drug conjugates: Recent advances in linker chemistry. *Acta Pharm. Sin. B* **2021**, *11*, 3889−3907.
(47) Kindermann, M.; George, N.; Johnsson, N.; Johnsson, K. Covalent and selective immobilization of fusion proteins. *J. Am. Chem. Soc.* **2003**, *125*, 7810−7811.
(48) Sokka, I. K.; Imlimthan, S.; Sarparanta, M.; Maaheimo, H.; Johansson, M. P.; Ekholm, F. S. Halogenation at the Phenylalanine Residue of Monomethyl Auristatin F Leads to a Favorable cis/trans Equilibrium and Retained Cytotoxicity. *Mol. Pharmaceutics* **2021**, *18*, 3125−3131.
(49) Johansson, M. P.; Maaheimo, H.; Ekholm, F. S. New insight on the structural features of the cytotoxic auristatins MMAE and MMAF revealed by combined NMR spectroscopy and quantum chemical modelling. *Sci. Rep.* **2017**, *7*, No. 15920.
(50) Acchione, M.; Kwon, H.; Jochheim, C. M.; Atkins, W. M. Impact of linker and conjugation chemistry on antigen binding, Fc receptor binding and thermal stability of model antibody-drug conjugates. *mAbs* **2012**, *4*, 362−372.
(51) Su, D.; Zhang, D. Linker design impacts antibody-drug conjugate pharmacokinetics and efficacy via modulating the stability and payload release efficiency. *Front. Pharmacol.* **2021**, *12*, No. 687926.
(52) Anami, Y.; Otani, Y.; Xiong, W.; Ha, S. Y.; Yamaguchi, A.; Rivera-Caraballo, K. A.; Zhang, N.; An, Z.; Kaur, B.; Tsuchikama, K. Homogeneity of antibody-drug conjugates critically impacts the therapeutic efficacy in brain tumors. *Cell Rep.* **2022**, *39*, No. 110839.


https://doi.org/10.1021/acsomega.2c06844
*ACS Omega* 2023, 8, 4026−4037